

Cosmic Web Classification through Stochastic Topological Ranking

Alejandro Palomino ^{1*}, Felipe L. Gómez-Cortés¹, Xiao-Dong Li^{2,3,4}, Jaime E. Forero-Romero ^{1,5†}

¹Departamento de Física, Universidad de los Andes, Cra. 1 No. 18A-10, Edificio Ip, CP 111711, Bogotá, Colombia

²School of Physics and Astronomy, Sun Yat-Sen University, Zhuhai 519082, China

³Peng Cheng Laboratory, No. 2, Xingke 1st Street, Shenzhen 518000, China

⁴CSST Science Center for the Guangdong–Hong Kong–Macau Greater Bay Area, SYSU, Zhuhai 519082, China

⁵Observatorio Astronómico, Universidad de los Andes, Cra. 1 No. 18A-10, Edificio H, CP 111711 Bogotá, Colombia

Accepted XXX. Received YYY; in original form ZZZ

ABSTRACT

This paper introduces ASTRA (Algorithm for Stochastic Topological RAnking), a novel method designed for the classification of galaxies into principal cosmic web structures—voids, sheets, filaments, and knots—especially tailored for large spectroscopic surveys. ASTRA utilizes observed data and a corresponding random catalog, generating probabilities for data and random points to belong to each cosmic web type. Extensive evaluation includes testing on datasets from N-body simulations (dark matter only and hydrodynamical) and observations, incorporating visual inspections and quantitative analyses of mass and volume filling fractions. ASTRA demonstrates proficiency in constructing void size function catalogs and is benchmarked against established cosmic web classification methods. Spatial correlations among cosmic web types are explored using 2-point correlation functions. ASTRA’s approach to the cosmic web holds promise for enhancing the retrieval of non-standard clustering statistics, thereby advancing the estimation of cosmological parameters. With simplicity, speed, and applicability across various datasets, ASTRA is a valuable tool in the quantitative study of the large-scale structure of the Universe.

Key words: methods: data analysis; cosmology: large-scale structure of Universe

1 INTRODUCTION

The large-scale distribution of galaxies in the Universe, known as the cosmic web, resembles a mesh of filaments spanning tens to hundreds of megaparsecs (Bond et al. 1996). The primary driver behind the evolution of the cosmic web is widely acknowledged to be the anisotropic process of gravitational collapse (Zel’dovich 1970). Small perturbations in the primordial density field evolve, giving rise to elongated filaments as they collapse along their intermediate and shorter axes (Springel et al. 2005). As such, the cosmic web holds crucial information about the distribution of matter-energy in the Universe and the underlying laws governing its evolution.

This suggests that accurately characterizing the cosmic web could serve as a powerful tool for probing both dark matter and dark energy within the standard cosmological model, as well as potentially shedding light on the nature of gravity. Due to these motivations, alongside the imperative to explore galaxy formation within a well-defined cosmological framework, a variety of methods with distinct foundations have emerged in recent decades. Currently, classification methods for the cosmic web can be broadly categorized into five distinct classes.

(i) **Methods Based on the Hessian (Geometric and Multiscale):** This category involves methods relying on the calculation of the Hessian of density, gravitational potential, or velocity field (Forero-

Romero et al. 2009; Hoffman et al. 2012). Implementing Hessian-based techniques requires spatial coordinates interpolation and the creation of a continuous field, typically achieved using Fourier transforms and smoothed with a Gaussian kernel. Geometric methods within this category establish connections between the morphology of density fields and the classification of points into cosmic structures. In contrast, multiscale methods use different scales when smoothing the field over which the Hessian is computed. The *Multiscale Morphology Filter* algorithm by Aragón-Calvo et al. (2007) is a prime example employing multiscale techniques.

(ii) **Graph-Based Methods:** Historically significant, these methods utilize graph theory principles to analyze matter distribution. The Minimum Spanning Tree (MST) algorithm is a notable example as it was one of the earliest approaches for studying filamentary structures (Barrow et al. 1985; Alpaslan et al. 2014). The MST is a tree-like structure that connects all the nodes of a given graph with the minimum total edge weight possible, finding the shortest path that connects all the nodes without forming any cycles. More recent examples include the β -skeleton (Fang et al. 2019), a geometric graph where edges connect points if the distance between them is not greater than a certain proportion (parameterized by β) of the distance to their nearest neighbor. This graph has been used to describe the cosmic web (Suárez-Pérez et al. 2021) and it is starting to be used to constrain cosmological parameters (Yin et al. 2024).

(iii) **Stochastic Methods:** Stochastic methods use statistical evolution of results derived from graphical or geometric concepts. An example is the approach outlined by Tempel, E. & Tamm, A. (2015),

* E-mail: a.palomino@uniandes.edu.co

† E-mail: je.forero@uniandes.edu.co

which classifies galaxies through hypothetical high-density cylinders with varying geometric configurations in each iteration. Stochastic methods offer an advantage in offsetting errors caused by data peculiarities and, like the method presented in this study, they do not require calculating a density field, utilizing only the coordinates of each point in the catalogs. However, this method is limited to finding filamentary structures.

(iv) Topological Methods: Similar to Hessian-based methods, topological methods aim to find general features in the morphology of filamentary structures. While Hessian-based methods focus on local search within geometric structures, topological methods study galaxy connections based on topological approaches. Two prime examples are the Disperse (Sousbie 2011) and the SpineWeb method (Aragón-Calvo et al. 2010), which use Morse theory and Delaunay tessellations to study the cosmic web. Another example is void finders that use Voronoi tessellations together with linking techniques to define aspherical voids (Sutter et al. 2015).

(v) Phase Space Methods: Phase space methods prioritize studying the dynamics of structure formation by analyzing the evolution of Phase Space generated initial conditions in simulations to a given epoch. An example is the method defined in Falck et al. (2012), which classifies points based on features found by studying the Lagrangian of the 6-dimensional phase space system. This method is limited to simulations where the positions and velocities of simulation particles are well determined both in the initial conditions and at another timestep of interest.

In this study, we introduce a new method called ASTRA (Algorithm for Stochastic Topological Ranking) designed for the classification of galaxies within the Cosmic Web. ASTRA innovates in three key aspects: it operates on the typical data structure derived from large scale structure catalogs from spectroscopic surveys, namely Cartesian coordinates computed from angular positions and redshifts and their corresponding random data distribution; it eliminates the need for interpolation, smoothing, or imposing fixed geometrical shapes on the data; and crucially, it has the capability to identify all four cosmic web types.

We structure this ASTRA presentation paper as follows. In §2 we describe the algorithm and the different applications of the ASTRA outputs. In §3 we describe the statistics and datasets that we are going to use to quantify ASTRA’s performance. We continue in §4 with the results together with a general discussion on ASTRA’s performance and capabilities before finally presenting our conclusions in the last section.

2 METHODOLOGY

The ASTRA method is a stochastic algorithm that classifies points in 3D space into one of four classes: voids, sheets, filaments, and knots. This classification is based on local computations made from a graph. The algorithm also needs as an input a random catalog of points that follows the number density distribution of the data points, hence its stochasticity.

2.1 Algorithm Description

The ASTRA method is a stochastic algorithm designed to classify points in 3D space into one of four categories: voids, sheets, filaments, and knots. This classification relies on local computations derived from a graph. The algorithm requires two input datasets: a set of data points and a set of random points. The stochastic nature

Table 1. Classification of points according to the distribution of neighbors given by the Delaunay triangulation.

Condition	Classification
$-1 \leq r \leq -0.9$	void
$-0.9 < r \leq 0$	sheet
$0 < r \leq 0.9$	filament
$0.9 < r \leq 1$	knot

of ASTRA is reflected in the need for a random catalog of points that follows the number density distribution of the data points.

The algorithm begins with the generation of two datasets: a set of data points and a set of random points. The ratio of the number of random points to the number of real points, denoted as $\rho = N_R/N_D$, is crucial. In our implementation, we generate an equal number of random points as real points ($\rho = 1$) to ensure consistent local mean point density in both datasets. This also necessitates that the volume spanned by the two datasets remains the same.

Subsequently, the merged catalog, comprising both real and randomly generated points, undergoes Delaunay triangulation. For each point in the merged catalog, we compute the number of connections to data points (N_D) and to random points (N_R). Using these quantities, we calculate the dimensionless parameter r for each point in the catalog, defined as:

$$r = \frac{N_D - N_R}{N_D + N_R}. \quad (1)$$

Positive r values indicate a greater number of connections to real points, while negative values indicate a higher number of connections to random points. Based on the value of r , each point in the merged catalog is classified into a web type according to predefined threshold values outlined in Table 1.

We adopt this formulation over an overdensity-based approach, such as $N_D/N_R - 1$, as it allows us to handle situations with high data point density where no random points, $N_R = 0$, are linked in the Delaunay triangulation.

As this classification procedure is applied to both real and random points, it is possible to identify random points classified as voids that correspond to the underdense regions in the real data.

The process can be iterated N times, with the random point distribution changing at each iteration, resulting in N distinct classifications for each data point. For these data points, the algorithm estimates the probability p_w of being classified into one of the four web elements (knot, filament, sheet, or void) as the ratio of the number of times the point was classified into each of these elements to the total number of iterations N .

Figure 1 offers a visual representation of the core functionality of the ASTRA algorithm in 2D. The left panel depicts the input data points as filled circles, while the middle panel illustrates the randomly generated points as empty circles. In the right panel, the Delaunay triangulation is shown, with continuous lines connecting data points and dashed lines linking at least one data point to one random point. By tallying the number of continuous and dashed line connections for each data point, the algorithm computes the r parameter, facilitating classification into one of the four web structures: voids, sheets, filaments, and knots.

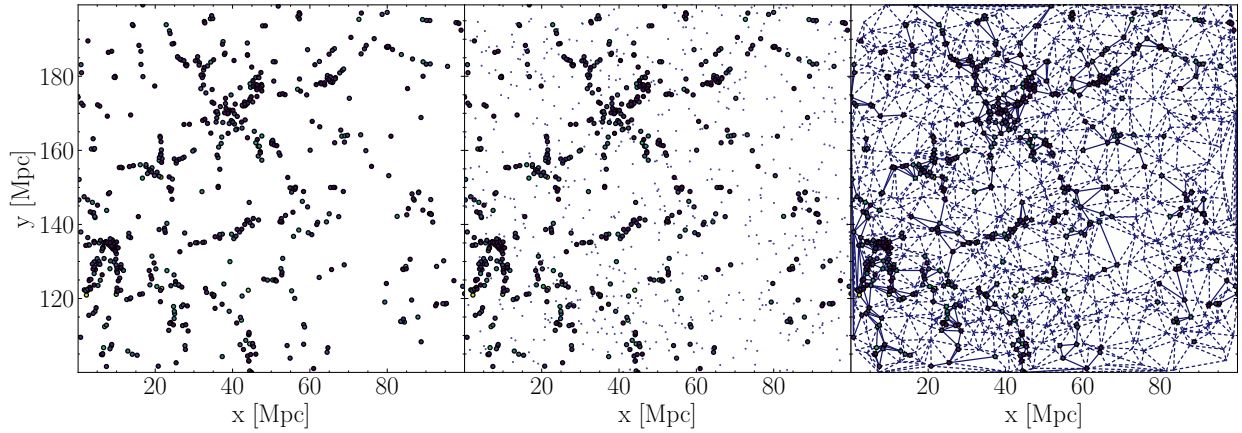


Figure 1. Illustration of the ASTRA method applied to a 2-dimensional dataset of 50 points. The left panel displays the input data points (black points). The center panel shows the randomly generated points uniformly distributed in the Monte Carlo iteration (blue points, smaller than the data points). The right panel depicts the Delaunay graph, with solid lines connecting two data points and dashed lines connecting at least one random point.

2.2 Applications of the ASTRA Outputs

The outputs of the ASTRA algorithm have various applications. Some of the ways in which the outputs will be utilized in this paper include:

- (i) By running the ASTRA procedure multiple times, the classification of a data or random point can be expressed as a probability of belonging to a specific web class. One can then select the web class with the highest probability.
- (ii) After a single iteration of ASTRA, data points with the same environment classification that are connected in the Delaunay graph can be grouped together. This grouping can be utilized to create catalogs of knots or filaments.
- (iii) Similarly, after a single iteration of ASTRA, random points with the same environment classification that are connected in the Delaunay graph can be grouped together. This grouping can be used to create catalogs of voids.
- (iv) Self and cross-correlation functions can be computed between data points with the same/different environments, random points with the same/different environments, and data points to random points with the same/different environments.

3 QUANTIFYING ASTRA

In this section, we aim to quantify the outputs of ASTRA in six different aspects:

- Perform a visual inspection for the different cosmic web types.
- Inspect the distributions for the r values and use classification entropy to quantify the robustness in assigning web types.
 - Quantify mass, luminosity, and volume distributions across web types.
 - Demonstrate how ASTRA can produce catalogs of the void size function.
 - Quantify the spatial correlations across web types using the 2-point auto and cross-correlation function.
 - Compare the ASTRA results against different published methods for cosmic web classification.

To accomplish these objectives, we utilize three different datasets as input to ASTRA.

3.1 Tracing the Cosmic Web (TCW)

The first simulated dataset used in this study is from the Tracing the Cosmic Web (TCW) comparison project (Libeskind et al. 2017). The simulation is a dark matter-only N-body simulation, with a box size of $200h^{-1}\text{Mpc}$ and 512^3 particles, using the Gadget-2 code (Springel 2005) and cosmological parameters of $h = 0.68$, $\Omega_M = 0.31$, $\Omega_\Lambda = 0.69$, $n_s = 0.96$, and $\sigma_8 = 0.82$. A dataset of 281,465 FOF dark matter haloes was obtained using a FOF algorithm Davis et al. (1985) with a linking length of $b = 0.2$ and a minimum of 20 particles for this analysis. This simulation is advantageous as it has already been analyzed by 11 different methods, which have also classified each point into one of the four cosmic structures.

3.2 Illustris-TNG

The second catalog of simulated data used in this study is from the Illustris-TNG project (Nelson et al. 2019), which includes simulations of dark matter from a redshift of $z = 127$ to $z = 0$ in boxes of sizes 50 Mpc, 100 Mpc, and 300 Mpc. The cosmological parameters used in these simulations are $h = 0.6774$, $\Omega_\Lambda = 0.6911$, $\Omega_M = 0.3089$, $\Omega_B = 0.0486$, $\sigma_8 = 0.8159$, $n_s = 0.9667$, and $H_0 = 100h \text{ km s}^{-1} \text{ Mpc}^{-1}$. For this study, we selected the TNG300-1 catalog, which has a box size of 300 Mpc, a redshift of $z = 0$, and 2500^3 particles. A filter was applied to select only those particles with a stellar mass above a certain threshold ($\log_{10}(M/M_\odot h^{-1}) > M_{\text{lim}}$, where $M_{\text{lim}} = 9$), resulting in a sample of 221,279 galaxies, with a density of $8 \times 10^{-3} \text{ Mpc}^{-3}$.

3.3 SDSS DR7

The third catalog used in our study is an observational data catalog from the Sloan Digital Sky Survey Data Release 7 (SDSS DR7) Abazajian et al. (2009). Specifically, we use data from the NYU Value-Added Galaxy Catalog Blanton et al. (2005), which includes large-scale structure samples constructed from SDSS data. Initially, we had 559,028 galaxies. To create a volume-limited sample, we applied cuts to the r-band magnitude and redshift. We selected all galaxies with an r-band magnitude of $M_r \leq -20$ and a redshift $z \leq 0.114$. We chose this magnitude limit to preserve all galaxies brighter than L_* Pan et al. (2012), as they reveal the structure of the cosmic web. Additionally, we selected galaxies in the declination

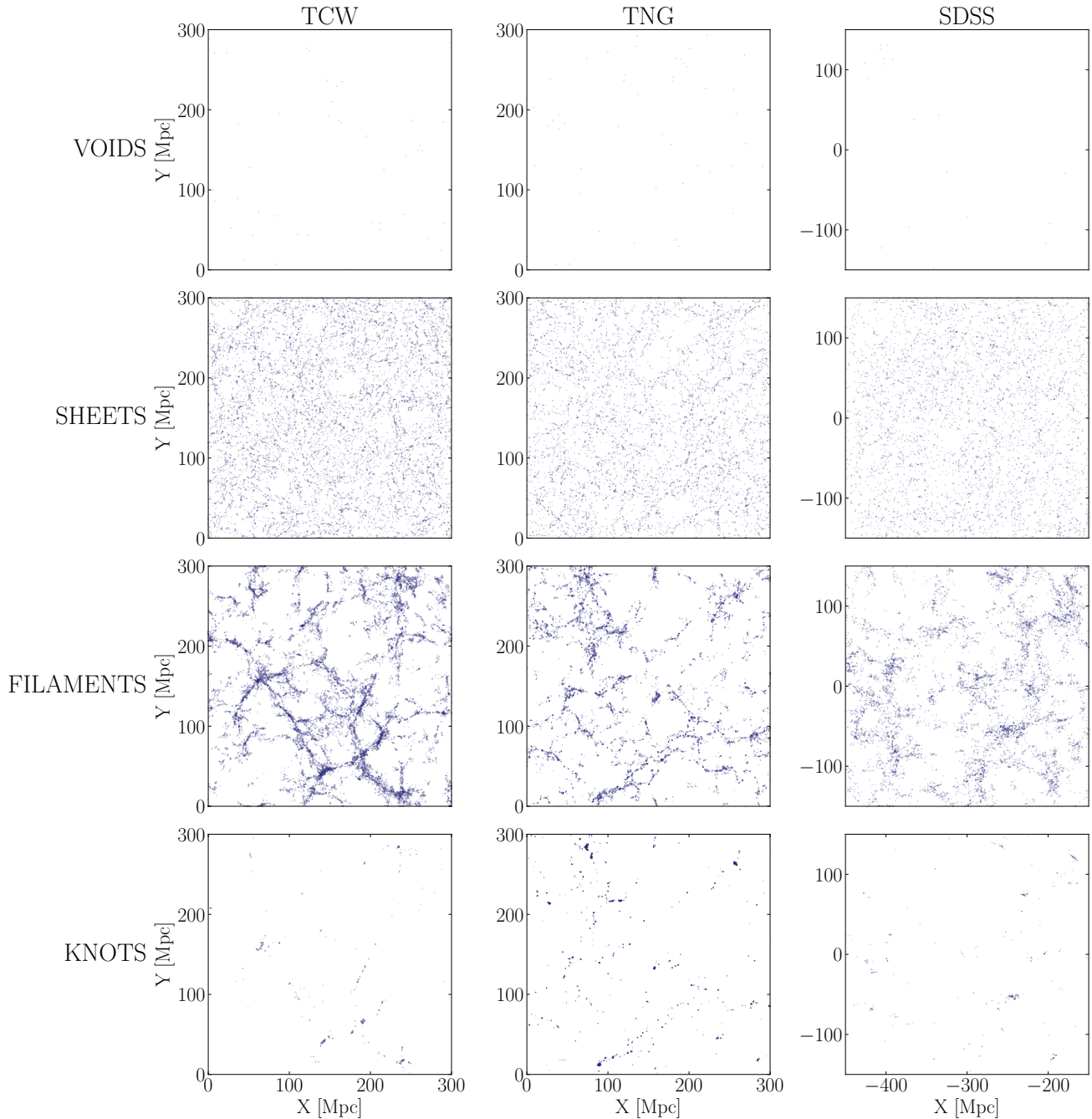


Figure 2. Plot of the classification given by ASTRA for each of the three data catalogs in the four galactic structures. The columns, from left to right, show the results obtained for TCW, TNG and SDSS, while the rows, from top to bottom, show the points belonging to each structure organized in ascending order of density; voids, sheets, filaments and knots. The image shows a z-slice that is 30 Mpc wide in the simulated catalogs, and 150 Mpc wide in SDSS. The structure of each of the painted points was chosen using the highest probability for each point after Monte Carlo iterations.

range between 0° and 50° , and right ascension range between 120° and 230° , resulting in a final sample of 90,655 galaxies.

4 RESULTS

4.1 Visual inspection

Figure 2 displays the results of the algorithm’s classification for the four cosmic web structures in three different catalogs, showing only

the points labeled as data. Moving from left to right, we see the simulated TCW and Illustris-TNG catalogs, followed by the observational SDSS-DR7 catalog. The structures, arranged from top to bottom in order of increasing average density, include voids, sheets, filaments, and knots. The visualized slice has a consistent size of 300 Mpc in width and 30 Mpc in depth for all cases.

These outcomes demonstrate the ability of ASTRA to produce the expected patterns across various inputs. The data points show distinct features, such as the highly stretched distribution for filaments, concentrated regions at the intersections of filaments for knots, a nearly

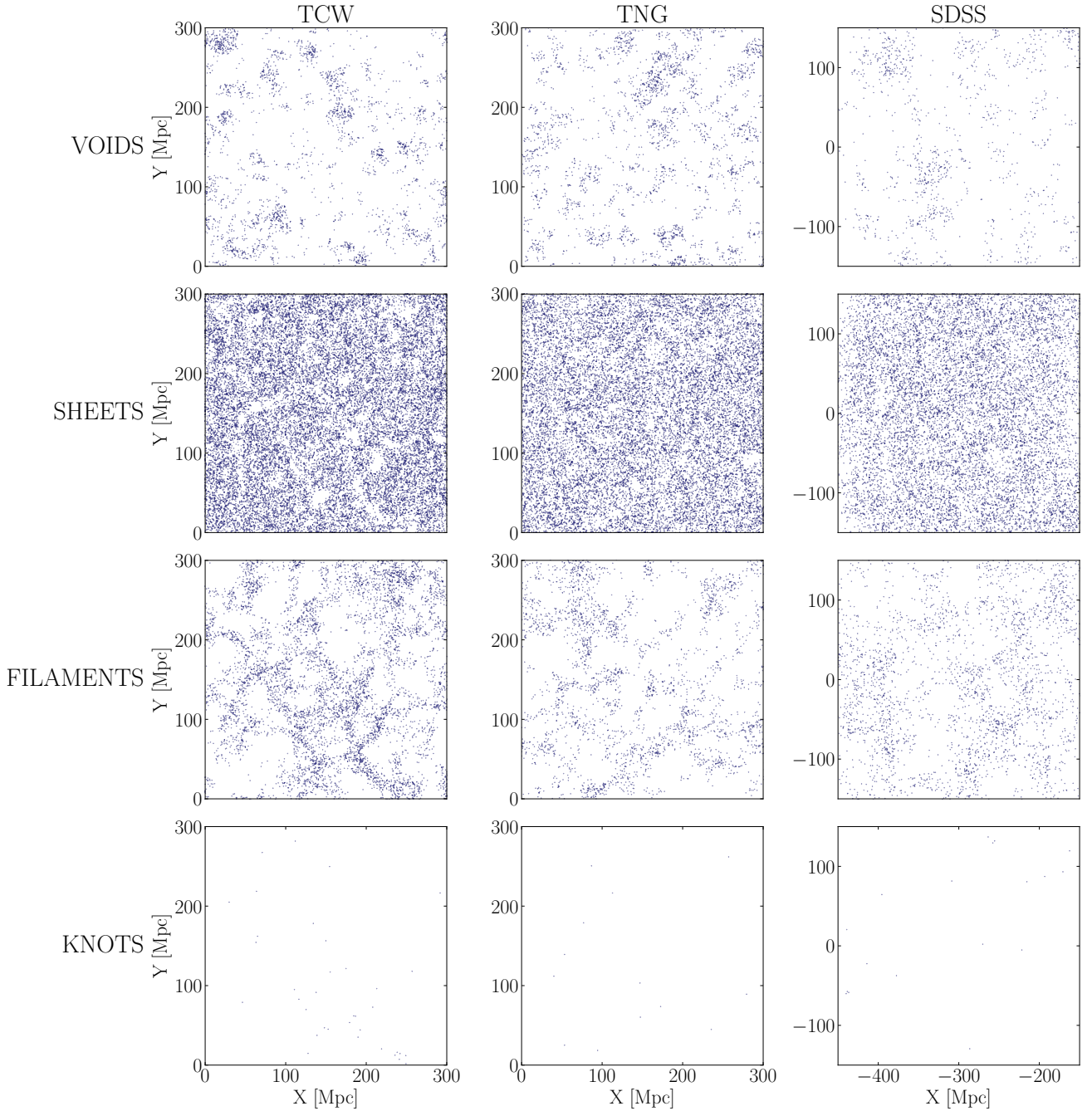


Figure 3. Plot of the classification given by ASTRA for the uniformly generated random points in each of the three data catalogs in a single Monte Carlo iteration in the four galactic structures. The columns, from left to right, show the results obtained for TCW, TNG and SDSS, while the rows, from top to bottom, show the points belonging to each structure organized in ascending order of density; voids, sheets, filaments and knots. The image shows the same z-slice as in Figure 2. The structure of each of the painted points was chosen with the results of the iteration classification.

uniform appearance for sheet points, and a highly sparse distribution for voids points.

Moving to Figure 3, the same slice as in Figure 2, we show the classification of random points in one Monte Carlo iteration. Here, the most notable observation is the clear presence of voids, contrasting with the filaments. Unlike the data points, random points classified as knots are sparse. The distribution of random points on sheets also remains spatially homogeneous across the different inputs.

4.2 Classification Entropy

Given that ASTRA can assign a probability for classification after multiple Monte Carlo iterations, we want to quantify the extent to which the uncertainty for the classification of a given point is large or small.

To this end, we use the normalized information entropy function:

$$H = -\frac{1}{\log_2 4} \sum_{i=1}^4 p_i \log_2(p_i) \quad (2)$$

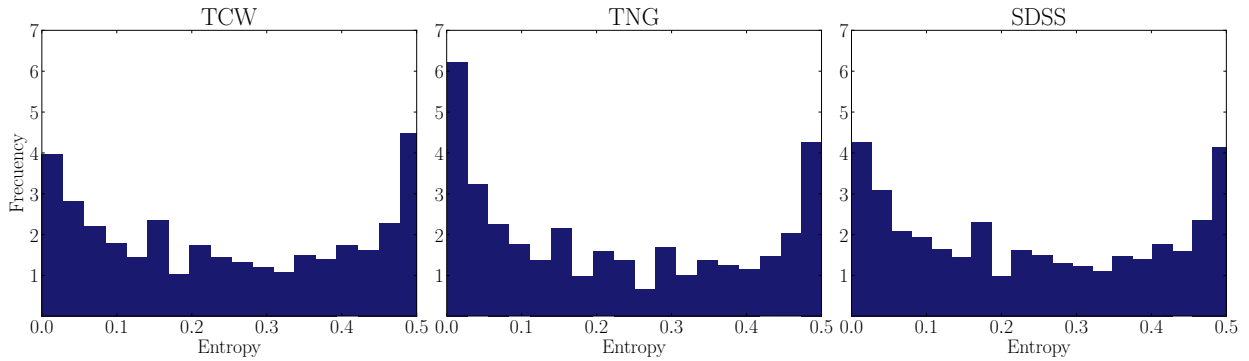


Figure 4. Probability Density Function for the entropy calculated on the real points of each of the three catalogs. In all cases the entropy is bound between 0 and 0.50, which indicates that, in general, the algorithm decides between two environments.

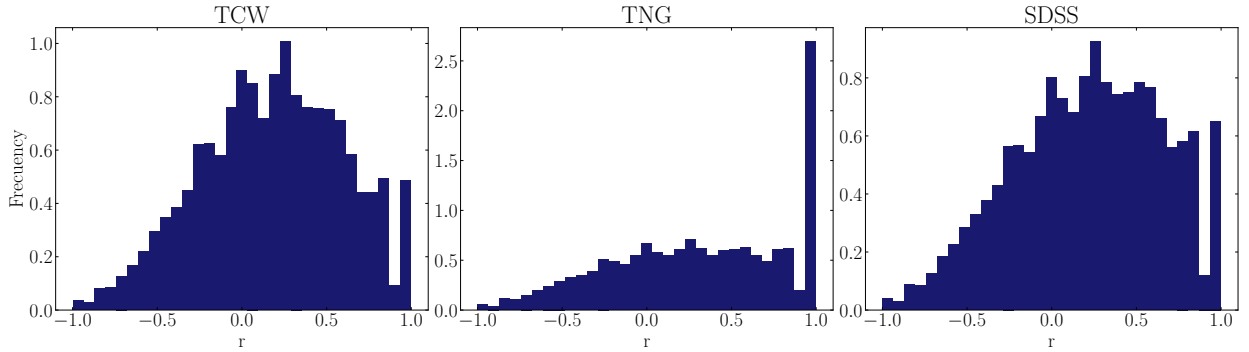


Figure 5. Probability Density Function for the parameter r on the real points of each of the three catalogs.

where p_i is the probability for each point to belong to each one of the four cosmic web environments.

H can range from 0 to 1. A value of 0 indicates that the algorithm is completely confident in its classification ($p_i = 1$ for a single i and 0 for the rest), meaning that in each iteration of the Monte Carlo method, the point was classified in the same structure. When two structures have equal probabilities of 0.5 ($p_i = p_j = 0.5$ for $i \neq j$), the entropy value is 0.5. The maximum entropy value of 1 is reached when all probabilities are equal and complete ignorance of the classification trends exists. Entropy values between 0 and 0.5 indicate that the classification must decide between a maximum of two environments for each point.

Figure 4 shows the estimated Probability Density Function (PDF) for the entropy over each of the real points in the three catalogs after 100 Monte Carlo iterations. The distributions are bound between 0 and 0.5, indicating that the algorithm's classifications only decide between two structures. This suggests that the r values do not significantly change across Monte Carlo iterations, which makes the classification robust. The small changes in r values simply shift the point across the classification threshold between two classes, but not across multiple classes.

In Figure 5, we show the estimated PDF for r on our three datasets. One of the first things that pops out is the large peak in the last bin, which actually corresponds to values of $r = 1$, indicating data points that are only connected to other data points. It is also noticeable that there is similarity between the r values of the TCW and SDSS catalogs, which was also seen in their entropy histograms (Figure 4). The increasing trend in the r is observed in the histograms until it reaches its peak around $r = 0.25$ in the region where the points are classified as filaments, then starts to decrease.

4.3 Mass and Luminosity Functions

We compute the fraction of points (data and random) that are found in each of the web types and then calculate the mean value and standard deviation for this fraction from 100 Monte Carlo iterations. The results are summarized in Table 2.

We use the fraction computed on the random points as an estimate of the volume filling fraction (VFF). These results are consistent across all three simulations, showing that in decreasing VFF values, we have: sheets, filaments, voids, and knots, with ranges between 69-73%, 15-23%, 6-11%, and 0.05-0.2%, respectively.

For the TCW and TNG simulations, we are able to compute the fraction of dark matter mass and stellar mass found in each structure, respectively. The relative ranking of mass fractions is consistent across the simulations. Most of the mass is found in filaments, followed by sheets, then knots, and finally voids. The percentages across the simulations vary. In the case of the DM simulation, almost 70% of the mass is found in filaments, while only 45% of the stellar mass is found in the same environments. This trend is inverted for knots, where 14% of the DM mass is found in haloes in these environments, whereas up to 34% of the stellar mass is found in the same type of environment.

Taking the ratio between the mass fraction and the volume fraction, one can achieve a mass density estimate (in units of the average mass density), which for the DM halo mass in TCW yields: 2×10^{-3} , 0.2, 3.0, and 100 for voids, sheets, filaments, and knots, respectively. For the stellar mass in TNG, it yields 6×10^{-3} , 0.3, 2.9, and 500 for the same environments. These values confirm the expected progression of increasing density for the density environments, which spans six orders of magnitude in the datasets we have used.

Table 2. Count and mass fraction of each structure in each of the three catalogs. For the count fraction we also compute it over the catalog computed on the random points, we use this as an estimate of the volume filling fraction of each environment. We compute the mean value and the standard deviation over 100 Monte Carlo iterations of ASTRA.

Count fraction				
Catalog	Voids	Sheets	Filaments	Knots
TCW	$(0.12 \pm 0.03)\%$	$(35.72 \pm 0.98)\%$	$(62.42 \pm 0.69)\%$	$(1.74 \pm 0.36)\%$
TNG	$(0.22 \pm 0.02)\%$	$(31.45 \pm 0.82)\%$	$(51.41 \pm 1.40)\%$	$(16.91 \pm 2.03)\%$
SDSS	$(0.14 \pm 0.04)\%$	$(33.89 \pm 0.98)\%$	$(63.58 \pm 0.63)\%$	$(2.38 \pm 0.46)\%$
TCW _{rand}	$(7.28 \pm 0.05)\%$	$(69.28 \pm 0.09)\%$	$(23.30 \pm 0.07)\%$	$(0.14 \pm 0.01)\%$
TNG _{rand}	$(11.54 \pm 0.09)\%$	$(73.13 \pm 0.11)\%$	$(15.26 \pm 0.07)\%$	$(0.07 \pm 0.01)\%$
SDSS _{rand}	$(6.78 \pm 0.09)\%$	$(72.60 \pm 0.13)\%$	$(20.45 \pm 0.08)\%$	$(0.17 \pm 0.01)\%$
Mass fraction				
TCW	$(0.020 \pm 0.001)\%$	$(15.00 \pm 1.08)\%$	$(70.38 \pm 3.15)\%$	$(14.60 \pm 3.80)\%$
TNG	$(0.08 \pm 0.01)\%$	$(20.07 \pm 0.71)\%$	$(44.92 \pm 2.37)\%$	$(34.93 \pm 2.99)\%$

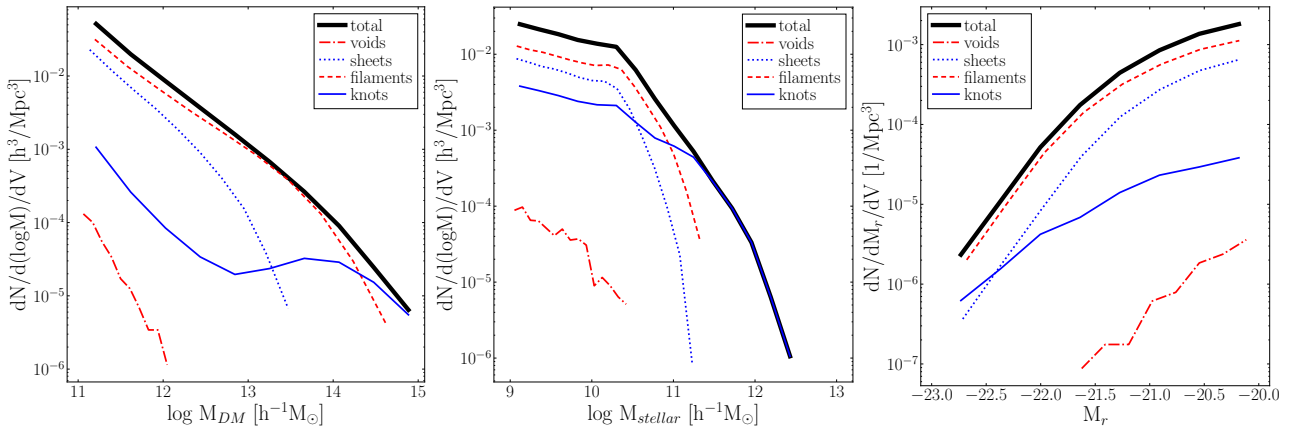


Figure 6. Different mass and luminosity functions for the different cosmic web environments. From left to right: dark matter halo mass on TCW, stellar mass on TNG and luminosity on SDSS.

To provide a broader picture, we show in Figure 6 different mass and luminosity functions split across environments. The main trends in these distributions are: 1. Objects classified as being in voids consistently show the lowest masses/luminosities. 2. Most of the objects are found in filaments, spanning all the mass/luminosity range. The exception is the objects from simulations, where the most massive systems are exclusively located in knots. 3. Sheets follow the mass/luminosity distribution of filaments, but their abundance is consistently lower than in filaments.

4.4 Void Catalogs

One distinguishing feature of ASTRA compared to other cosmic web identification methods is its capability to assign random points to a web environment. This functionality enables the definition of void points as part of the random set and facilitates the identification of void random points connected in the Delaunay graph.

This straightforward grouping algorithm allows for the creation of void catalogs in each iteration. Various properties can then be computed from the points within each void, including the number of points, inertia tensor, and eigenvalues. Since voids typically lack spherical symmetry, their radius, R_{void} , can be estimated as the square root of the average of the three inertia tensor eigenvalues.

Figure 7 illustrates the PDF for the logarithm of void radius, considering only voids traced with a minimum of 4 random points. The overall shape of these void size functions aligns with expected theoretical trends (Sheth & van de Weygaert 2004) and findings from other void detection methods Shandarin et al. (2006). A detailed comparison with different parameterizations and void detection methods is reserved for future investigation.

Voids have also been extensively studied and utilized to constrain cosmological parameters by leveraging the void size function and spatial cross-correlation between void centers and galaxies (Verza et al. 2019; Nadathur et al. 2019; Contarini et al. 2023). However, the precision of measurements utilizing spatial cross-correlation is limited by a numerical challenge: while the number of galaxies used could be on the order of 10^6 , the number of void positions for cross-correlation is typically on the order of 10^3 . This disparity of three orders of magnitude introduces noise into the numerical estimation of cross-correlation, involving the construction of a 2D histogram of relative distances for approximately 10^9 galaxy-void pairs.

In our approach, we utilize random points that sample voids, not just their centers. With the number of random points matching the number of galaxies, and approximately 10% of random points tracing voids, the galaxy sample of 10^6 can be cross-correlated with 10^5 positions representing voids. This increase of two orders of magnitude

in the number of galaxy-void pairs used for the 2D cross-correlation function enhances precision. While a thorough examination of this method's potential for constraining cosmological parameters is reserved for future work, we explore its feasibility by analyzing the results of measuring the auto and cross-correlation functions for different web types in both data and random samples, as measured by ASTRA.

4.5 2-point cross correlations

The clustering of galaxies in each web-type can be quantified using the 2-point correlation function (2PCF), which characterizes the excess probability of finding a galaxy within a given distance of another galaxy compared to a random distribution (Davis & Peebles 1983). In the observed universe, the galaxy distribution appears anisotropic due to radial velocity perturbations introduced by peculiar velocities of galaxies. This motivates the use of two coordinates, s and μ , to describe galaxy separations, where s represents the pair separation along the line of sight, and μ is the cosine of the angle between the vector connecting the galaxies and the observer's line of sight.

A commonly used estimator for the 2PCF (Landy & Szalay 1993) involves a random point distribution as a reference and is described as:

$$\xi(s, \mu) = \frac{DD - 2DR + RR}{RR}, \quad (3)$$

where DD is the number of galaxy pairs in the s, μ bin, DR is the number of galaxy-random pairs, and RR is the number of random-random pairs.

To differentiate different angular components in the 2PCF, the function can be projected into Legendre polynomials to compute the multipole moments defined by:

$$\xi_\ell(s) = \frac{2\ell + 1}{2} \int_{-1}^1 \xi(s, \mu) P_\ell(\mu) d\mu. \quad (4)$$

In this paper, we focus on the monopole, $\xi_0(s)$, and the quadrupole, $\xi_2(s)$, measured on the volume-limited data from SDSS presented in previous sections. No weights are applied to galaxies to account for observational systematics, and no Feldman-Kaiser-Peacock weights (Feldman et al. 1994) are used to correct for variations in the number density of galaxies. The correlation functions are measured in 61 μ bins from -1 to 1 and 21 radial bins from 0.1 to 80 Mpc. Randoms are used with 10 times more points than the original galaxy catalog.

We also measure cross-correlations between two different samples, D_1 and D_2 , using:

$$\xi(s, \mu) = \frac{D_1 D_2 - D_1 R_2 - D_2 R_1 + R_1 R_2}{R_1 R_2}, \quad (5)$$

where R_1 and R_2 are two different random sets.

In our case, we use four different samples: data-sheets, data-filaments, random-sheets, and random-voids, corresponding to samples in their respective datasets. We avoid using samples with a low number of points such as data-voids, data-knots, and random-knots. These datasets allow us to compute six different cross-correlations and four different self-correlation functions.

The main results for these correlations are shown in Figure 8. The monopole exhibits its largest amplitudes for the auto-correlation of data-filaments, random-voids, and their cross-correlation. Furthermore, these correlations show a distinctive transitional scale around 20 Mpc. The next high-amplitude cross-correlation is found for data-sheets and random-voids, also with a transitional scale around 15-20 Mpc. Some of the quadrupoles show large anisotropies, the largest

being found for the auto-correlation of data-filaments and their cross-correlation with random-voids, especially for scales larger than 40 Mpc. This might be due to the fact that filaments and voids are expected to show large redshift space distortions which influence their selection effect when identified in redshift space.

We anticipate that a data vector composed by the concatenation of all the self and cross-correlation results could be used to constrain cosmological parameters (Paillas et al. 2023). This involves a complex process that includes predicting the expected covariance matrix for all observables, taking into account observational biases, instrumental limitations, and efficiently exploring the cosmological parameter space. Such a process is beyond the scope of this paper and is left for future work.

4.6 Comparison Against Other Cosmic Web Finding Methods

With the aim of gaining deeper insight into ASTRA's capabilities, we present a comparative analysis against other cosmic web identification methods. Our goal is to identify the method that most closely resembles ASTRA's results based on the TCW simulation, incorporating findings from various cosmic web detectors.

Table 3 provides an overview of the methods employed in the TCW project, for which public data exists on the classification of FOF DM haloes. The table outlines the web types each method can categorize, the types of input data it can handle (dense, from simulations, or sparse, from observations), and whether it operates on a grid-based system. To assess the similarity between the results obtained using different methods and those obtained using ASTRA, we computed confusion matrices and calculated the weighted average F1 score across different structures.

Figure 9 presents the confusion matrices for the 11 methods compared to the results of all methods in the TCW paper (Libeskind et al. 2017). Two key observations emerge from this figure. Firstly, the most significant discrepancies in classification occur for voids, where ASTRA often classifies DM halos as sheets, contrary to other methods. Secondly, the highest level of agreement in classification generally occurs for filaments. The classification accuracy across the six methods that categorize into four structures typically follows a decreasing order: filaments, sheets, knots, and voids.

To provide a quantitative evaluation of these observations, we employed the F1 score, a commonly used metric in statistical analysis to assess classification accuracy. The F1 score is calculated as the harmonic mean of precision and recall, where precision denotes the ratio of true positive results to the total number of positive results found, and recall represents the ratio of true positive results to the total number of results that should have been classified as positive. For methods classifying three or more classes, we utilized the F1 score weighted by the number of instances in each class.

The last column in Table 3 summarizes the F1 score for each comparison. Among methods producing a four-type classification, NEXUS yields the most similar results to ASTRA, with an F1 score of 0.65. For three-type classification, the highest F1 score is obtained in the comparison with DisPerSE, scoring 0.68. When comparing against filament classifiers, the best result is achieved in the comparison with FINE, yielding an F1 score of 0.69. Moreover, the highest level of agreement across methods and cosmic web environments is observed for filaments in the V-web algorithm, with 94% of the galaxies classified as filaments also identified by ASTRA.

From this comparison, we conclude that ASTRA stands out among other methods for its unique ability to classify all web types, handle both dense and sparse data points, and operate without requiring a

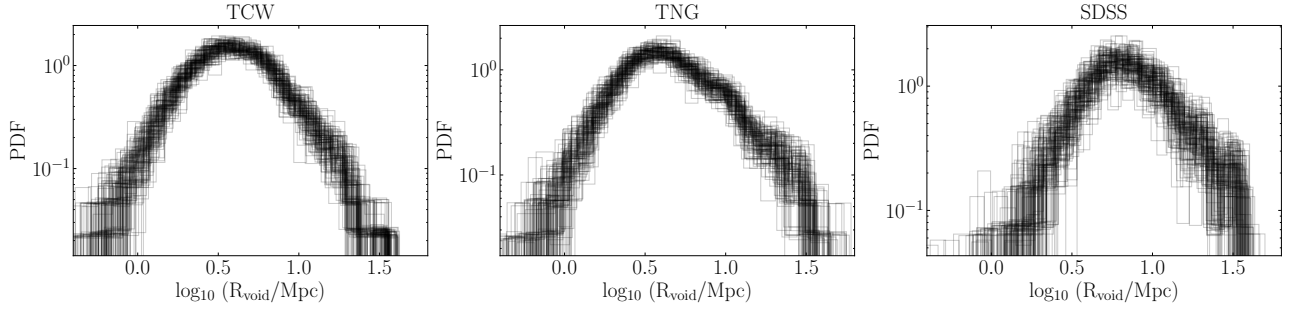


Figure 7. Void size functions. There are 100 different lines in each panel, each line corresponds to a different iteration of the ASTRA algorithm. Each panel, from left to right, corresponds to the TCW, TNG and SDSS datasets. We keep voids that are traced with at least four random points.

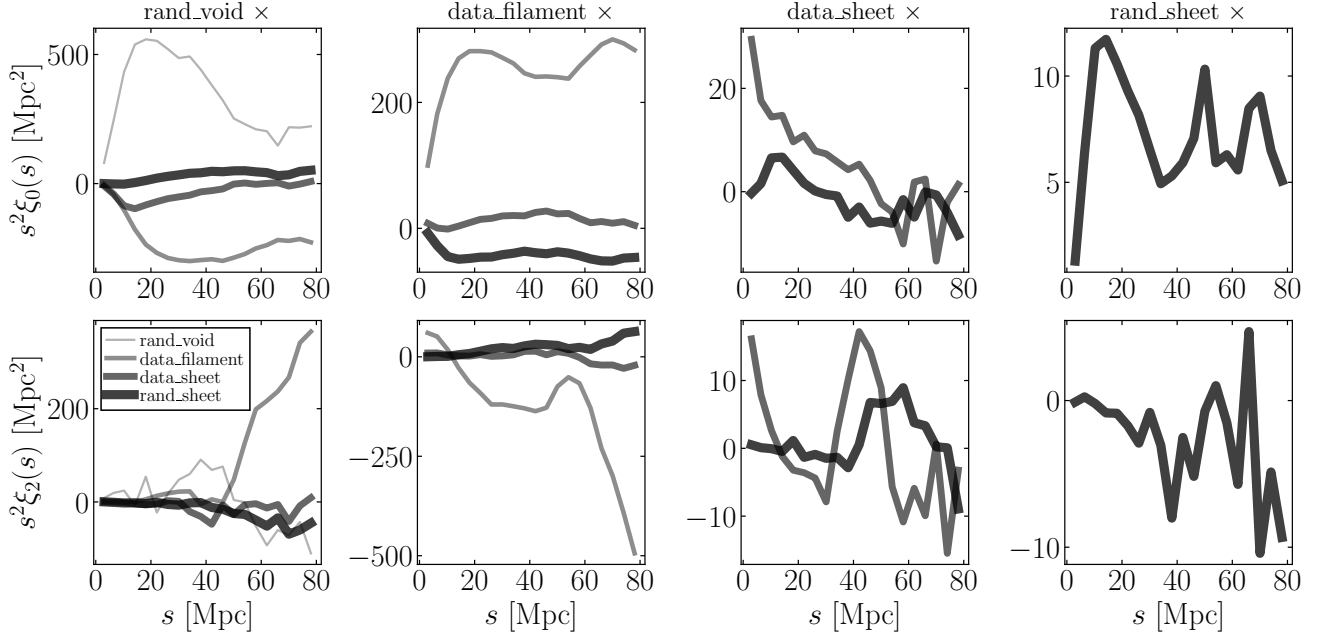


Figure 8. Two-point correlation function multipoles measured using the SDSS DR7 catalogue. Each column represents a different point set (random void, data filament, data sheet and random sheet), while the inset displays the corresponding dataset against which the correlation functions are computed. We observe from this analysis that the most prominent signals arise from the auto-correlations of random voids and data filaments, along with their respective cross-correlations.

Table 3. Overview of the methods used in the *Tracing the Cosmic Web* (Libeskind et al. 2017). The Input distinguishes between dense (typically DM computational particles from an N-body simulation) and sparse (typically DM haloes or galaxies).

Method	Web types	Input	Grid based	Main Reference	F1-score
ASTRA	all	sparse	No	This paper	1.0
MSWA	all	dense	No	Ramachandra & Shandarin (2015)	0.55
T-web	all	dense	Yes	Forero-Romero et al. (2009)	0.59
V-web	all	dense	Yes	Hoffman et al. (2012)	0.36
CLASSIC	all	dense	Yes	Kitaura & Angulo (2012)	0.37
NEXUS +	all	dense	Yes	Cautun et al. (2012)	0.65
ORIGAMI	all	dense	No	Falck et al. (2012)	0.35
DisPerSE	all except knots	sparse	No	Sousbie (2011)	0.68
SpineWeb	all except knots	dense	Yes	Aragón-Calvo et al. (2010)	0.55
MMF-2	all except knots	dense	Yes	Aragón-Calvo et al. (2007)	0.64
Bisous	filaments	sparse	No	Tempel et al. (2014)	0.41
FINE	filaments	sparse	Yes	González & Padilla (2010)	0.69

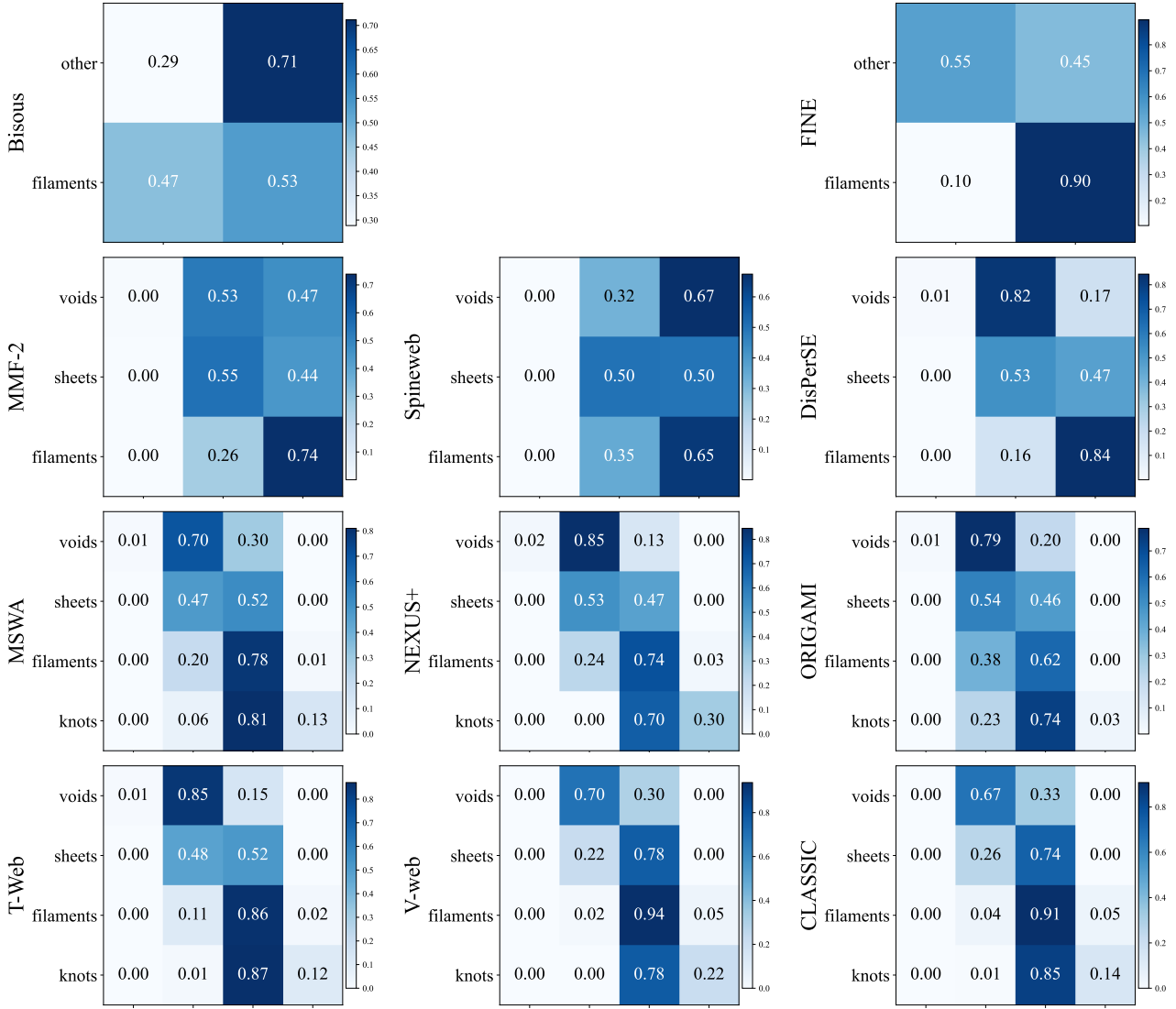


Figure 9. Confusion matrices built by comparing the results given by ASTRA on the TCW catalog against those given by the methods cited in Table 3. The first row corresponds to the methods that can only classify dark matter halos in filaments, the second those that can classify them in all environments except knots, and the last two rows correspond to the remaining 6, which can, like ASTRA, classify the points in each of the four structures.

grid. Furthermore, the haloes classified as filaments appear to be the most agreed-upon result when compared against other methods.

5 CONCLUSIONS

On the scale of Megaparsecs, the galaxy distribution shows a pattern of interconnected structures known as the cosmic web, that is usually classified into four primary morphological types: voids, sheets, filaments, and knots. Here we introduced ASTRA, a novel method adept at utilizing sparse 3D point-based data to assign a probability of classification into a specific cosmic web type for each data point.

ASTRA integrates a random catalog with the input data catalog, leveraging Delaunay graph construction to evaluate the connectivity between actual data points and random samples. Through iterative refinement using distinct random catalogs, ASTRA computes probabilities for each point, indicating its likelihood of belonging to a particular cosmic web type.

To validate ASTRA's capabilities, we applied it to three diverse

datasets: a catalog of haloes from a dark matter-only N-body simulation (Libeskind et al. 2017), a catalog of subhaloes from a hydrodynamical simulation (Nelson et al. 2019), and galaxy catalogs from the Sloan Digital Sky Survey (SDSS) (Abazajian et al. 2009).

Visual inspection and statistical analysis of the results yield the following insights:

- Visual inspection confirms expected trends, with knots predominantly situated in dense regions, filaments connecting these knots, sheets appearing in regions of average density with less clustering than filaments, and voids corresponding to underdense regions anti-correlated with filaments.
- The highest volume filling fraction, estimated from random points, is observed in sheets, while knots exhibit the lowest filling fraction. The mass filling fraction, estimated only for simulations, is highest in filaments and lowest in voids, with a density ranking from voids to knots.
- Stellar/dark matter halo mass segregation aligns with expectations, with voids predominantly hosting low-mass systems and knots

hosting large-mass systems. Filaments and knots exhibit similar distributions, with a predominance of low-mass systems.

- ASTRA facilitates the construction of void size abundance functions, revealing expected trends with peaks around void radii of 3-7 Mpc.

- Significant amplitudes and features in the monopole and quadrupole of auto and cross-correlation functions suggest potential for constraining cosmological parameters at special transitional spatial scales.

- In comparisons with other cosmic web finders, ASTRA demonstrates remarkable consistency in identifying halos belonging to filaments.

In summary, our results showcase ASTRA's effectiveness in classifying points in the cosmic web. The method is characterized by its simplicity, speed, and independence from density grid calculations or Gaussian smoothing, making it an attractive option for future cosmic web studies. The consistency of results across different datasets underscores ASTRA's versatility, suggesting applicability across a wide range of data types. Moreover, ASTRA's ability to classify random points enhances our understanding of cosmic web structure and its underlying properties.

Overall, ASTRA presents promising capabilities for cosmic web classification and analysis, offering valuable insights into the large-scale structure of the universe. We anticipate its application to contribute significantly to ongoing and future extragalactic spectroscopic surveys, aiding in uncovering new correlations between physical processes and galaxy formation within the cosmic web and advancing our understanding of cosmological models.

ACKNOWLEDGEMENTS

DATA AVAILABILITY

The data underlying this article are available in <https://github.com/forero/DelaunayASTRA>

REFERENCES

Abazajian, K. N., Adelman-McCarthy, J. K., Agüeros, M. A., Allam, S. S., Prieto, C. A., An, D., Anderson, K. S. J., Anderson, S. F., Annis, J., Bahcall, N. A., Bailer-Jones, C. A. L., Barentine, J. C., Bassett, B. A., Becker, A. C., Beers, T. C., Bell, E. F., Belokurov, V., Berlind, A. A., Berman, E. F., Bernardi, M., Bickerton, S. J., Bizyaev, D., Blakeslee, J. P., Blanton, M. R., Bochanski, J. J., Boroski, W. N., Brewington, H. J., Brinchmann, J., Brinkmann, J., Brunner, R. J., Budavári, T., Carey, L. N., Carliles, S., Carr, M. A., Castander, F. J., Cinabro, D., Connolly, A. J., Csabai, I., Cunha, C. E., Czarapata, P. C., Davenport, J. R. A., de Haas, E., Dilday, B., Doi, M., Eisenstein, D. J., Evans, M. L., Evans, N. W., Fan, X., Friedman, S. D., Frieman, J. A., Fukugita, M., Gänsicke, B. T., Gates, E., Gillespie, B., Gilmore, G., Gonzalez, B., Gonzalez, C. F., Grebel, E. K., Gunn, J. E., Györy, Z., Hall, P. B., Harding, P., Harris, F. H., Harvanek, M., Hawley, S. L., Hayes, J. J. E., Heckman, T. M., Hendry, J. S., Hennessy, G. S., Hindsley, R. B., Hoblitt, J., Hogan, C. J., Hogg, D. W., Holtzman, J. A., Hyde, J. B., ichi Ichikawa, S., Ichikawa, T., Im, M., Ivezić, Ž., Jester, S., Jiang, L., Johnson, J. A., Jorgensen, A. M., Jurić, M., Kent, S. M., Kessler, R., Kleinman, S. J., Knapp, G. R., Konishi, K., Kron, R. G., Krzesinski, J., Kuropatkin, N., Lampeitl, H., Lebedeva, S., Lee, M. G., Lee, Y. S., Leger, R. F., Lépine, S., Li, N., Lima, M., Lin, H., Long, D. C., Loomis, C. P., Loveday, J., Lupton, R. H., Magnier, E., Malanushenko, O., Malanushenko, V., Mandelbaum, R., Margon, B., Marriner, J. P., Martínez-Delgado, D., Matsubara, T., McGehee, P. M., McKay, T. A., Meiksin, A., Morrison, H. L., Mullally, F., Munn, J. A., Murphy, T., Nash, T., Neboit, A., Neilsen, E. H., Newberg,

H. J., Newman, P. R., Nichol, R. C., Nicinski, T., Nieto-Santisteban, M., Nitta, A., Okamura, S., Oravetz, D. J., Ostriker, J. P., Owen, R., Padmanabhan, N., Pan, K., Park, C., Pauls, G., Peoples, J., Percival, W. J., Pier, J. R., Pope, A. C., Pourbaix, D., Price, P. A., Purger, N., Quinn, T., Raddick, M. J., Fiorentin, P. R., Richards, G. T., Richmond, M. W., Riess, A. G., Rix, H.-W., Rockosi, C. M., Sako, M., Schlegel, D. J., Schneider, D. P., Scholz, R.-D., Schreiber, M. R., Schwobe, A. D., Seljak, U., Sesar, B., Sheldon, E., Shimasaku, K., Sibley, V. C., Simmons, A. E., Sivarani, T., Smith, J. A., Smith, M. C., Smolčić, V., Snedden, S. A., Stebbins, A., Steinmetz, M., Stoughton, C., Strauss, M. A., SubbaRao, M., Suto, Y., Szalay, A. S., Szapudi, I., Szkody, P., Tanaka, M., Tegmark, M., Teodoro, L. F. A., Thakar, A. R., Tremonti, C. A., Tucker, D. L., Uomoto, A., Berk, D. E. V., Vandenberg, J., Vidrih, S., Vogeley, M. S., Voges, W., Vogt, N. P., Wadadekar, Y., Watters, S., Weinberg, D. H., West, A. A., White, S. D. M., Wilhite, B. C., Wonders, A. C., Yanny, B., Yocum, D. R., York, D. G., Zehavi, I., Zibetti, S., & Zucker, D. B., 2009. THE SEVENTH DATA RELEASE OF THE SLOAN DIGITAL SKY SURVEY, *The Astrophysical Journal Supplement Series*, **182**(2), 543–558.

Alpaslan, M., Robotham, A. S. G., Driver, S., Norberg, P., Baldry, I., Bauer, A. E., Bland-Hawthorn, J., Brown, M., Cluver, M., Colless, M., Foster, C., Hopkins, A., Van Kampen, E., Kelvin, L., Lara-Lopez, M. A., Liske, J., Lopez-Sanchez, A. R., Loveday, J., McNaught-Roberts, T., Merson, A., & Pimblett, K., 2014. Galaxy And Mass Assembly (GAMA): the large-scale structure of galaxies and comparison to mock universes, *MNRAS*, **438**(1), 177–194.

Aragón-Calvo, M. A., Jones, B. J. T., van de Weygaert, R., & van der Hulst, J. M., 2007. The multiscale morphology filter: identifying and extracting spatial patterns in the galaxy distribution, *A&A*, **474**(1), 315–338.

Aragón-Calvo, M. A., Platen, E., van de Weygaert, R., & Szalay, A. S., 2010. The Spine of the Cosmic Web, *ApJ*, **723**(1), 364–382.

Barrow, J. D., Bhavsar, S. P., & Sonoda, D. H., 1985. Minimal spanning trees, filaments and galaxy clustering, *MNRAS*, **216**, 17–35.

Blanton, M. R., Schlegel, D. J., Strauss, M. A., Brinkmann, J., Finkbeiner, D., Fukugita, M., Gunn, J. E., Hogg, D. W., Ivezić, Ž., Knapp, G. R., Lupton, R. H., Munn, J. A., Schneider, D. P., Tegmark, M., & Zehavi, I., 2005. New York University Value-Added Galaxy Catalog: A Galaxy Catalog Based on New Public Surveys, *AJ*, **129**(6), 2562–2578.

Bond, J. R., Kofman, L., & Pogosyan, D., 1996. How filaments of galaxies are woven into the cosmic web, *Nature*, **380**(6575), 603–606.

Cautun, M., van de Weygaert, R., & Jones, B. J. T., 2012. NEXUS: tracing the cosmic web connection, *Monthly Notices of the Royal Astronomical Society*, **429**(2), 1286–1308.

Contarini, S., Pisani, A., Hamaus, N., Marulli, F., Moscardini, L., & Baldi, M., 2023. Cosmological Constraints from the BOSS DR12 Void Size Function, *ApJ*, **953**(1), 46.

Davis, M. & Peebles, P. J. E., 1983. A survey of galaxy redshifts. V. The two-point position and velocity correlations., *ApJ*, **267**, 465–482.

Davis, M., Efstathiou, G., Frenk, C. S., & White, S. D. M., 1985. The evolution of large-scale structure in a universe dominated by cold dark matter, *ApJ*, **292**, 371–394.

Falck, B. L., Neyrinck, M. C., & Szalay, A. S., 2012. ORIGAMI: DELINEATING HALOS USING PHASE-SPACE FOLDS, *The Astrophysical Journal*, **754**(2), 126.

Fang, F., Forero-Romero, J., Rossi, G., Li, X.-D., & Feng, L.-L., 2019. β -Skeleton analysis of the cosmic web, *MNRAS*, **485**(4), 5276–5284.

Feldman, H. A., Kaiser, N., & Peacock, J. A., 1994. Power-Spectrum Analysis of Three-dimensional Redshift Surveys, *ApJ*, **426**, 23.

Forero-Romero, J. E., Hoffman, Y., Gottlöber, S., Klypin, A., & Yepes, G., 2009. A dynamical classification of the cosmic web, *MNRAS*, **396**(3), 1815–1824.

González, R. E. & Padilla, N. D., 2010. Automated detection of filaments in the large-scale structure of the Universe, *Monthly Notices of the Royal Astronomical Society*, **407**(3), 1449–1463.

Hoffman, Y., Metuki, O., Yepes, G., Gottlöber, S., Forero-Romero, J. E., Libeskind, N. I., & Knebe, A., 2012. A kinematic classification of the cosmic web, *Monthly Notices of the Royal Astronomical Society*, **425**(3), 2049–2057.

- Kitaura, F.-S. & Angulo, R. E., 2012. Linearization with cosmological perturbation theory, *Monthly Notices of the Royal Astronomical Society*, **425**(4), 2443–2454.
- Landy, S. D. & Szalay, A. S., 1993. Bias and Variance of Angular Correlation Functions, *ApJ*, **412**, 64.
- Libeskind, N. I., van de Weygaert, R., Cautun, M., Falck, B., Tempel, E., Abel, T., Alpaslan, M., Aragón-Calvo, M. A., Forero-Romero, J. E., Gonzalez, R., Gottlöber, S., Hahn, O., Hellwing, W. A., Hoffman, Y., Jones, B. J. T., Kitaura, F., Knebe, A., Manti, S., Neyrinck, M., Nuza, S. E., Padilla, N., Platen, E., Ramachandra, N., Robotham, A., Saar, E., Shandarin, S., Steinmetz, M., Stoica, R. S., Sousbie, T., & Yepes, G., 2017. Tracing the cosmic web, *Monthly Notices of the Royal Astronomical Society*, **473**(1), 1195–1217.
- Nadathur, S., Carter, P. M., Percival, W. J., Winther, H. A., & Bautista, J. E., 2019. Beyond BAO: Improving cosmological constraints from BOSS data with measurement of the void-galaxy cross-correlation, *Phys. Rev. D*, **100**(2), 023504.
- Nelson, D., Springel, V., Pillepich, A., Rodriguez-Gomez, V., Torrey, P., Genel, S., Vogelsberger, M., Pakmor, R., Marinacci, F., Weinberger, R., Kelley, L., Lovell, M., Diemer, B., & Hernquist, L., 2019. The IllustrisTNG simulations: public data release, *Computational Astrophysics and Cosmology*, **6**(1), 2.
- Paillas, E., Cuesta-Lazaro, C., Zarrouk, P., Cai, Y.-C., Percival, W. J., Nadathur, S., Pinon, M., de Mattia, A., & Beutler, F., 2023. Constraining $\nu\Lambda$ CDM with density-split clustering, *MNRAS*, **522**(1), 606–625.
- Pan, D. C., Vogeley, M. S., Hoyle, F., Choi, Y.-Y., & Park, C., 2012. Cosmic voids in Sloan Digital Sky Survey Data Release 7, *Monthly Notices of the Royal Astronomical Society*, **421**(2), 926–934.
- Ramachandra, N. S. & Shandarin, S. F., 2015. Multi-stream portrait of the cosmic web, *Monthly Notices of the Royal Astronomical Society*, **452**(2), 1643–1653.
- Shandarin, S., Feldman, H. A., Heitmann, K., & Habib, S., 2006. Shapes and sizes of voids in the Lambda cold dark matter universe: excursion set approach, *MNRAS*, **367**(4), 1629–1640.
- Sheth, R. K. & van de Weygaert, R., 2004. A hierarchy of voids: much ado about nothing, *MNRAS*, **350**(2), 517–538.
- Sousbie, T., 2011. The persistent cosmic web and its filamentary structure – I. Theory and implementation, *Monthly Notices of the Royal Astronomical Society*, **414**(1), 350–383.
- Springel, V., 2005. The cosmological simulation code gadget-2, *Monthly Notices of the Royal Astronomical Society*, **364**(4), 1105–1134.
- Springel, V., White, S., Jenkins, A., Frenk, C., Yoshida, N., Gao, L., Navarro, J., Thacker, R., Croton, D., Helly, J., Peacock, J., Cole, S., Thomas, P., Couchman, H., Evrard, A., Colberg, J., & Pearce, F., 2005. Simulations of the formation, evolution and clustering of galaxies and quasars, *Nature*, **435**(7042), 629–636.
- Suárez-Pérez, J. F., Camargo, Y., Li, X.-D., & Forero-Romero, J. E., 2021. The Four Cosmic Tidal Web Elements from the β -skeleton, *ApJ*, **922**(2), 204.
- Sutter, P. M., Lavaux, G., Hamaus, N., Pisani, A., Wandelt, B. D., Warren, M., Villaescusa-Navarro, F., Zivick, P., Mao, Q., & Thompson, B. B., 2015. VIDE: The Void IDentification and Examination toolkit, *Astronomy and Computing*, **9**, 1–9.
- Tempel, E., Stoica, R. S., Martínez, V. J., Liivamägi, L. J., Castellan, G., & Saar, E., 2014. Detecting filamentary pattern in the cosmic web: a catalogue of filaments for the SDSS, *MNRAS*, **438**(4), 3465–3482.
- Tempel, E. & Tamm, A., 2015. Galaxy pairs align with galactic filaments, *A&A*, **576**, L5.
- Verza, G., Pisani, A., Carbone, C., Hamaus, N., & Guzzo, L., 2019. The void size function in dynamical dark energy cosmologies, *J. Cosmology Astropart. Phys.*, **2019**(12), 040.
- Yin, F., Ding, J., Lai, L., Zhang, W., Xiao, L., Wang, Z., Forero-Romero, J., Zhang, L., & Li, X.-D., 2024. Improving SDSS Cosmological Constraints through β -Skeleton Weighted Correlation Functions, *arXiv e-prints*, p. arXiv:2403.14165.
- Zel'dovich, Y. B., 1970. Gravitational instability: An approximate theory for large density perturbations., *A&A*, **5**, 84–89.

This paper has been typeset from a $\text{\TeX}/\text{\LaTeX}$ file prepared by the author.